Investigation of Risk Factors Contributing to the Occurrence of Posterior Rib Fractures

Francisco J. Lopez-Valdes, Manuel Valdano, Ema Jokubaityte, Amaya Palacios Weiss, Carlos J. Carpintero Rubio, Rohan Govardhan, Sanjay Baladaniya, Jeya Padmanaban

Abstract Posterior rib fractures are clinically important because they are associated with severe thoracic trauma and increased risk of intrathoracic complications, yet their biomechanical etiology remains incompletely understood. This study investigated factors contributing to posterior rib fractures by combining three complementary data sources: selected real-world crash cases from RASSI and CIREN, computed tomography analyses of four PMHS that sustained posterior rib fractures in frontal impacts, and a parametric simulation study using the VIVA+ human body model. The real-world cases showed that posterior rib fractures may occur both after direct posterior loading and in crashes dominated by distributed thoracic compression without clear posterior contact. In the PMHS analyses, Hounsfield unit measurements at the costovertebral and costotransverse joints were generally higher than those of vertebral cancellous bone, and elevated values often coincided with fractured levels. In the simulations, increased stiffness at the rib-spine connections and intervertebral joints shifted strain toward rib regions closer to the spine and increased model-predicted rib fracture risk. These findings support the hypothesis that local thoracic stiffening may contribute to posterior rib fractures under compressive loading. The results are exploratory and support further validation using larger datasets and subject-specific modeling.

Keywords Injury mechanisms, Joint stiffness, Posterior rib fractures, Real-world frontal impacts, VIVA+.

I. INTRODUCTION

Rib fractures are a common manifestation of thoracic trauma. Their anatomical location is associated with both the injury mechanism and the clinical prognosis. Clinical studies have shown that rib fractures are present in 10% to 20% of all patients with blunt trauma, with an average of 9.8 fractures per patient in severe injuries [1]. In general, lateral fractures are the most frequent in overall thoracic trauma [2]; however, in high-energy trauma, the proportion of posterolateral fractures increases significantly [3]. Hospital-based observational studies have shown that posterior rib fractures are significantly more frequent in patients with associated intrathoracic or intra-abdominal injuries (46.2% vs. 17.2%), further supporting their association with greater injury severity [4].

From a clinical perspective, the posterior location of rib fractures is particularly relevant because of its proximity to critical anatomical structures, such as the thoracic aorta, intercostal vessels, and the vertebral column. This location entails a higher risk of complications such as hemothorax, vascular injury, or neurological damage, as well as increased mortality [5]. In addition, biomechanical studies have shown that collapse of the posterior ribs produces a greater reduction in thoracic volume than collapse of the anterior ribs, thereby negatively affecting respiratory function and substantially increasing the risk of mortality [6]. The treatment of posterior rib fractures follows the general principles of thoracic trauma management [7]. Nevertheless, posterior fracture location often requires more intensive management, particularly in cases of multiple or displaced fractures, and ventilatory support and, in selected situations, surgical stabilisation of the chest wall may become necessary [8]. The prognosis of these injuries depends on multiple factors: (1) the total number of fractures; (2) the presence of displacement; (3) patient age; (4) associated injuries; and (5) the posterior location of the fractures [9–11].

The etiology of posterior rib fractures is closely linked to high-energy traumatic mechanisms, with motor vehicle crashes representing one of the main contexts described. Current experimental and observational evidence indicates that the distribution of rib fractures depends on both impact direction and the restraint systems used. In frontal collisions involving seat belt use, fractures tend to occur along the belt path, predominantly in the anterior and anterolateral regions [3][12]. However, as crash severity increases, the injury pattern extends to the lateral and posterolateral regions, suggesting that involvement of the posterior rib cage corresponds to greater

F.J. Lopez-Valdes (fjlvaldes@comillas.edu, +34 91 542 28 00), M. Valdano and C.J. Carpintero Rubio are Professors and Researchers, E. Jokubaityte is a PhD candidate, at MOBIOS Lab, Institute for Research in Technology, Universidad Pontificia Comillas. A. Palacios Weiss is Head of the Radiology Dept., Fundacion Hospitalarias, Madrid, Spain. R.Govardhan is a Project Manager, S.Baladaniya is a RASSI- Senior Automotive Injury Analyst, and J. Padmanaban is President and Founder of JP Research India Pvt. Ltd. (e-mail: contact@jpri.in; tel: +91-7066027860), registered in Pune, Maharashtra, India.

energy transfer to the thorax [12].

Among the most relevant predisposing factors for these injuries, the existing literature suggests the following:

- Advanced age: older patients are more susceptible to rib fractures, even in lower-severity impacts, because of reduced bone density and diminished thoracic elasticity [2][3].
- Impact severity: increasing delta-V is correlated with a greater number of fractures and with more complex fracture patterns, including posterior locations [13].
- Restraint system configuration: the combination of seat belt and airbag redistributes forces and generates more diffuse loading patterns that may affect the posterolateral region [12].
- Thoracic biomechanics: the posterior region of the ribs has lower mobility and greater stiffness because of its vertebral attachment, which makes it more vulnerable to injury under intense compressive loading [14–15].

In conclusion, posterior rib fractures constitute a marker of high-energy thoracic trauma and are associated with greater clinical severity compared with fractures in other locations. The available evidence supports their role as a relevant prognostic factor in the context of thoracic trauma. Thus, this study combines data from real-world collisions, from the analysis of computer tomography (CT) of Post Mortem Human Subjects (PMHS) that received posterior rib fractures being exposed to frontal impacts and results obtained with the VIVA+ Human Body Model (HBM) to discuss and suggest relevant factors contributing to the etiology of posterior rib fractures.

II. METHODS

Three different datasets were used. First, a handful of real-world impact cases in which one participant had sustained posterior rib fractures were considered. Second, analyses of CT images from PMHS sustaining posterior rib fractures after participating in a frontal impact. Last, a parametric study using the VIVA+ HBM was used to explore the influence of increased rib joint stiffness in the distribution of strain along the rib.

Real-world Cases

Selected case studies from the Road Accident Sampling System–India (RASSI) and the National Automotive Sampling System Crashworthiness Data System/Crash Injury Research and Engineering Network (NASS CDS/CIREN) were reviewed in this paper. The real-world cases were selected to illustrate plausible injury mechanisms, not to estimate incidence

Road Accident Sampling System- India (RASSI)

RASSI is India's only nationally representative sample of crashes based on in-depth investigations conducted across the country. The RASSI database is based on a statistical stratified sampling methodology and contains data of over 8,500 crashes occurred on Indian roads from 2011 to date. RASSI is a collaborative effort between multiple stakeholders including government agencies and automobile manufacturers and component manufacturers. During RASSI crash investigations, researchers collect a set of 600+ data points covering scene characteristics, vehicle damage, injury data, occupant data, and crash contributing factors. RASSI data also includes interviews, accident reconstruction data where vehicle speeds, avoidance distance, Delta-V, etc. are calculated using the PC-Crash accident reconstruction software.(*PC-Crash, Dr. Steffan Datentechnik*).

Researchers collect detailed medical records and hospital data of crash victims, capturing comprehensive information on sustained injuries. In addition, evidence of occupant contact points within/outside the vehicle are documented during crash investigations to support injury mechanism analysis. The medical record data collected on the site data are then analysed by trained specialists certified in the Abbreviated Injury Scale (AIS) coding techniques by the Association for the Advancement of Automotive Medicine (AAAM). Using AIS methodology, each injury is coded, enabling the derivation of injury severity metrics such as Maximum AIS (MAIS). This structured injury analysis is further correlated with crash reconstruction outputs, occupant kinematics, physical evidence, and documented occupant contact points. By analysing injury patterns, mechanisms, kinematics, and contact interactions, the relationship between vehicle and injuries sustained by occupants is established.

A unique feature of RASSI is the ability to project national estimates based on the sample of crashes collected. A stratified sampling system has been developed to derive national estimates from sample of crashes and national statistics published by MoRTH (Ministry of Road Transport), India. The methodology used to derive national estimates for RASSI data is based on the NASS-CDS sampling weight methodology developed by NHTSA,US and sampling weight methodology developed for German In-Depth Accident Study (GIDAS) data in Germany [16].

The Crash Injury Research and Engineering Network (CIREN)

CIREN is administered by the National Highway Traffic Safety Administration (NHTSA) in the United States. It is an in-depth crash investigation program designed to elucidate the relationships among crash circumstances, vehicle characteristics, occupant factors, and injury outcomes. CIREN integrates prospective case enrollment, structured data acquisition, and multidisciplinary medical-engineering analysis to determine injury causation in real-world motor-vehicle collisions.

CIREN cases are identified at five Level I trauma centres that manage large numbers of motor-vehicle crash victims. Eligible patients are approached for informed consent, after which CIREN teams obtain access to de-identified medical records and digital radiology datasets. Each medical centre team is led by trauma surgeons or emergency physicians and includes trained crash investigators and research coordinators.

Crash investigators document vehicle, environmental, and occupant circumstances using standardized NHTSA protocols. These procedures include vehicle inspections, scene documentation, and technical crash reconstruction. Parallel to this process, medical staff perform comprehensive abstraction of injuries, treatments, and imaging findings, and all imaging is archived for research use. Engineering centre at academic research institutions lead the biomechanical assessment of each case. Mechanical engineers (specialised in human injury biomechanics) evaluate impact conditions, contact locations, applied forces, and injury mechanisms. Some cases incorporate computational reconstructions to refine the biomechanical assessment.

Publicly accessible cases date back to 2004 and contain de-identified crash, occupant, and injury information, including detailed crash reconstructions and comprehensive medical injury profiles.

Analyses of PMHS Computed Tomography (CT)

The pre-test CT from four PMHS that sustained posterior rib fractures after being exposed to either 40 km/h or 50 km/h frontal impacts in an acceleration sled [17] were analysed (Table I). The tests used a simplified vehicle environment with a semi-rigid seat, reclined seat back, contemporary 3-point belt, and no airbag [18]. The density of the tissues in the CT images can be estimated based on the measurement of the attenuation of the radiation received. This measurement is expressed using Hounsfield units (HU), a scale in which water is defined as having 0 HU and air is defined as -1000 HU. Typical values for cancellous bone are between 100 and 300 HU, while soft tissues can be found roughly between 20 and 80 HU.

TABLE I
PMHS CHARACTERISTICS

Subject	Sex	Age	Cause of death	Number and location of posterior rib fractures
1	Male	64	Gastric disease	Total: 3. Left aspect, ribs: 5, 6, 7
2	Male	63	Cardiac insufficiency	Total: 6. Right aspect, ribs: 3; left aspect, ribs: 2, 3, 4, 5, 6
3	Male	72	Cardiac arrest	Total: 10. Right aspect, ribs: 7, 8, 9; left aspect, ribs: 4, 6, 7, 8, 9, 10, 11
4	Male	65	Bladder cancer	Total: 1. Left aspect: 11

For these subjects, several measurements were taken at the different thoracic vertebral levels. First, a measurement of the HU at a central location of each thoracic vertebrae was taken to be used as a reference for a measurement of the HU of cancellous bone for the specific subject and vertebral level. Then, three measurements at different heights in the sagittal plane were taken for each costo-vertebral (CV) and costo-transverse (CTv) joints. These two joints connect the ribs to the vertebrae as shown in Fig. A.5. The average of the HU values obtained in the three measurements per joint was considered an estimate of the ossification level of the joint. In addition, the location, number and type of rib fractures sustained by these four PMHS were documented during the post-test autopsy performed at MOBIOS Lab (Universidad Pontificia Comillas).

Computational Modeling

The study employed four publicly available load cases from the VIVA+ HBM Validation Suite: a frontal sled test [19], a frontal hub impactor test [20], a lateral hub impactor test [21], and belt-driven tabletop loading [22]. Illustrations of the simulation load cases have been included in the Appendix. The VIVA+ HBM thoracic response has been described already in the literature and is considered appropriate to analyse the human response to thoracic loading [23].

The following descriptions refer to their implementation in simulation rather than the exact experimental configurations, as documented in the VIVA+ Validation Suite. The Crandall case is a full-body sled test with a prescribed 30 km/h deceleration pulse, in which the pelvis and lower extremities are constrained and distributed anterior thoracic loading is applied through a three-point restraint system. The Kroell case is a frontal rigid impactor test to the mid-sternum using a 152 mm diameter, 23 kg impactor in simulation at 4.3 and 6.7 m/s, producing localised anterior-posterior thoracic compression with high rib deflection. The Viano case applies a lateral rigid impactor to the thorax at the level of the xiphoid process, producing side chest deformation at 4.4 and 6.5 m/s. The Kent tabletop configuration applies to either a single diagonal belt or two diagonal belts (X-belt), generating respectively more concentrated and more distributed thoracic loading without global body acceleration.

One severity configuration was used for each load case, corresponding to the highest severity available within the validation datasets: 6.7 m/s for the frontal rigid impactor and X-belt loading for the tabletop tests. However, the validated frontal sled and lateral thorax impactor configurations were not injurious enough to produce significant rib fracture risk. Therefore, the Crandall pulse was scaled to correspond to a 45 km/h impact, and the Viano lateral impactor velocity was increased to 9.8 m/s. These choices ensured measurable rib strain and fracture risk for the sensitivity assessment while preserving the original loading definitions.

Each loading condition was simulated using the default VIVA+ model as the baseline configuration. The effects of additional stiffness in the costovertebral (CV) joint, the intervertebral discs, and their combination were then assessed. The intervertebral disc is modeled as a general non-linear six-degree-of-freedom beam. Increased disc stiffness was implemented by scaling by a factor of 10 the force-deformation and moment-rotation curves for all thoracic vertebrae and all beam axes. The costovertebral joints are represented as spherical joints, with stiffness defined by moment-rotation relationships. Increased CV stiffness was implemented by scaling by a factor of 10 the three moment-rotation curves defining the joint response. The analysis focused on the distribution of strain along each rib and the potential increase in rib fracture risk.

III. RESULTS

Real-world Cases

Case 1: RASSI 91-2019-002—0113

This crash case involves a fatally-injured, belted, 42-year-old, male driver of a 2019 Maruti Suzuki Wagon R four-door small hatch, which was involved in a frontal collision with a truck. There were four other occupants (all unbelted) in the car and all four sustained fatal injuries. This head-on vehicle collision occurred on a rural, two-lane, two-way, dry asphalt roadway. The estimated delta-v for the passenger car was 90 km/h, while it was only 8 km/h for the heavy truck due to the mass differences. Both vehicles received almost a pure frontal impact (Principal direction of force (PDOF): 1 o'clock, passenger car; 12o'clock, truck). Within the scope of this manuscript, only the injuries sustained by the fatally injured driver of the passenger car will be discussed.

The 42-year-old male driver was restrained by a three-point lap and shoulder belt not incorporating pretensioners, and by a frontal airbag, which deployed in the collision as shown in Fig. 1. The vertical position of the D-ring was not adjustable for this vehicle. A summary of all the injuries sustained by the driver is provided in Fig. 2, while the detailed description of the thoracic and abdominal injuries sustained by the driver is presented in Table II. After the investigation of the case, the posterior rib injuries of the driver were attributed to the direct contact with the seatback that was pushed forward by the unbelted occupants travelling in the rear seat of the vehicle.

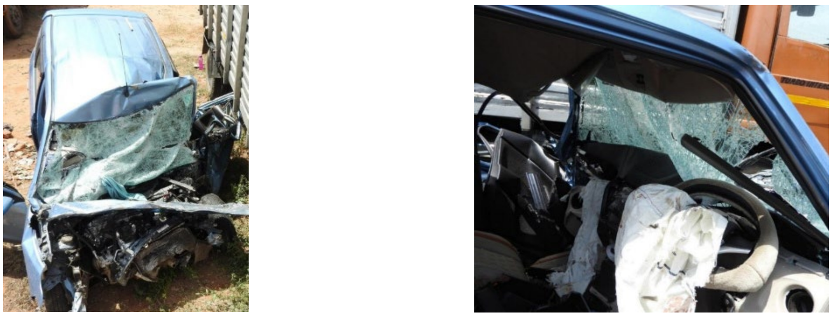

Fig. 1. Pictures from the exterior and interior (driver seat) of the relevant passenger car involved in Case 1.

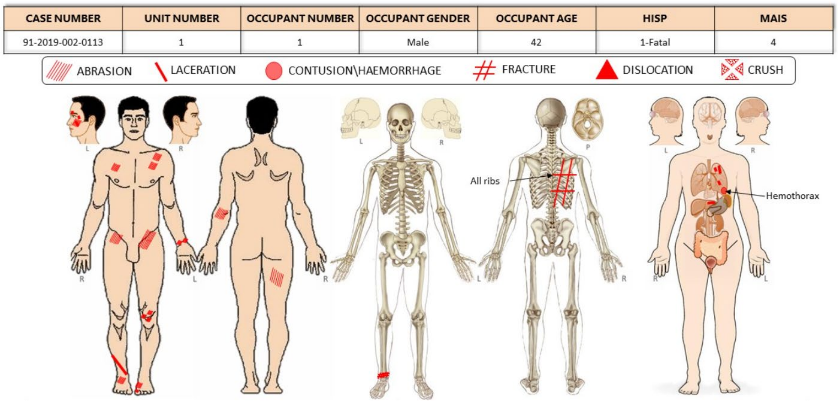

Fig. 2. Summary of injuries sustained by driver in Case 1.

TABLE II

CASE1. DRIVER THORACIC AND ABDOMINAL INJURIES (AIS 2+)

Inj #	Injury Description	AIS Code	Aspect
1	Laceration over back of upper and lower lobes, left lung	441432.4	Left
2	Left pleural cavity containing 800 ml of blood	442300.3	Left
3	Rib fractures, posterior, left side	450203.3	Left, posterior
4	Liver laceration, left lobe, 8 cm	541822.2	Unknown

Case 2: RASSI 91-2023-011-0196

This crash case involves a fatally-injured, belted, 28-year-old, male driver of a 2000 Maruti Suzuki Zen four-door mini hatch, which was primarily involved in a frontal-oblique collision with a roadside concrete structure on the left-side ditch. There were three other occupants (all unbelted) in the car, and all other occupants sustained minor injuries. This head-on vehicle collision occurred on a four-lane divided, dry asphalt national highway at night. The estimated impact speed against the rigid concrete structure was 32 km/h. The vehicle was not equipped with airbags, and the three-point seat belt was not pretensioned. The seatback angle of the driver's seat remained upright, and there was no evidence of hard contact of the driver with the seatback. The vertical position of the driver´s seat belt was not adjustable in this vehicle. Pictures of the car and the interior are provided in Fig. 3.,Fig. 4 and Table III include the summary of all injuries sustained by the driver and details of thoracic and abdominal AIS2+ injuries. This evidence suggests that the posterior rib fractures were caused by the distribution of deformation over the chest of the occupant without a direct impact to the posterior region of the rib cage.

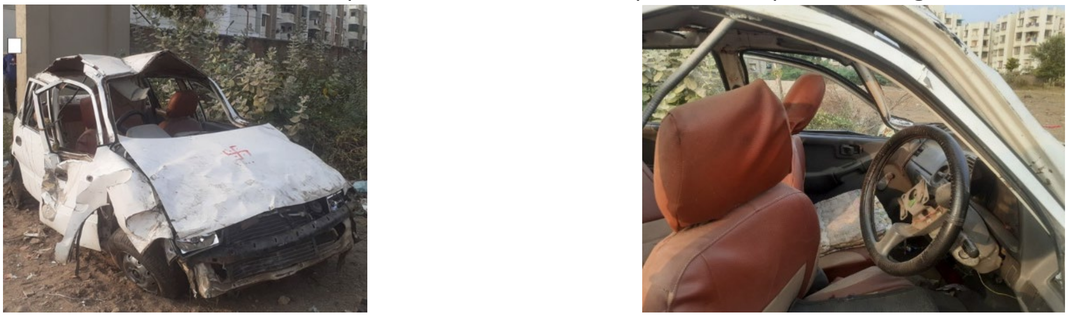

Fig. 3. Pictures from the car involved in Case 2.

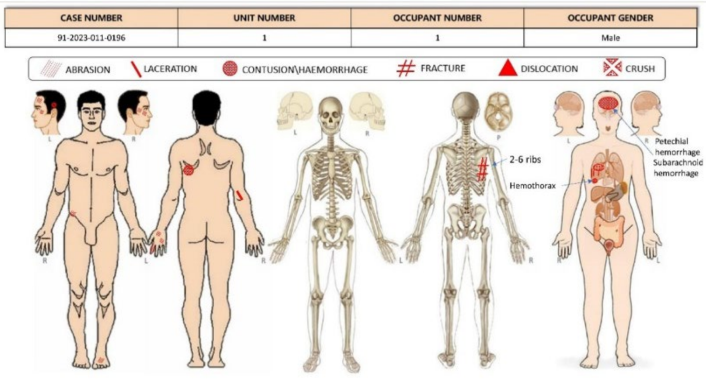

Fig. 4. Summary of injuries sustained by driver in Case 2.

TABLE III

CASE2. DRIVER THORACIC AND ABDOMINAL INJURIES (AIS 2+)

Inj #	Injury Description	AIS Code	Aspect
1	Right lung, middle lobe, contusion	441406.2	Right
2	Right hemothorax, 100 ml	442200.3	Right
3	Fracture, posterior lateral aspect of 2nd to 6th ribs, right	450203.3	Right, posterior
4	Superficial laceration oblique, right lobe, liver	541822.2	Right, lateral

Case 3: CIREN CASE 584

This crash case involves a moderately-injured, belted, 183 cm, 77 kg, 72-year-old, male driver of a 2019 Mercedes C300 four-door sedan, which was primarily involved in a frontal collision with a large tree. The driver of Vehicle 1 was restrained by his three-point lap and shoulder belt (with retractor pretensioner), and the vehicle was equipped with advanced frontal airbags, first and second-row seat backrest-mounted hip/torso airbags, and roof rail-mounted curtain airbags. As a result of the impact, the driver's steering wheel, knee bolster, and roof rail-mounted curtain airbags deployed. Pictures of the car and the interior are shown in Fig. 5. The driver sustained moderate injuries (summarised in Fig. 6). The driver seat was reported to be between the mid-track to rear positions. In post-crash images the seatback appears slightly reclined. The shoulder belt anchorage was reported to be in full-upright position. The posterior rib injuries were attributed to the contact with the left door panel (left forward upper quadrant) with the contributing factor of high delta-v and involving a compression mechanism. This causation scenario was considered certain, and the evidence was a non-optimal posture biased forward oblique by the slope of the road and the 1st event. The AIS information from the abdominal and thoracic AIS2+ injuries are provided in Table IV.

Fig. 5. Pictures of the exterior and interior of the vehicle in Case 3.

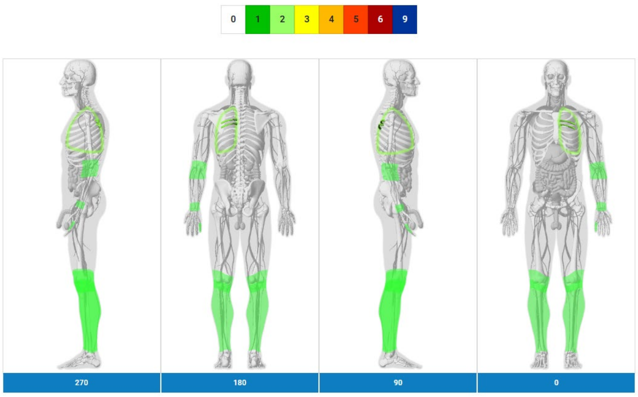

Fig. 6. Summary of injuries sustained by driver in Case 3.

TABLE IV

CASE3. DRIVER THORACIC AND ABDOMINAL INJURIES (AIS 2+)

Inj #	Injury Description	AIS Code	Localizer
1	Thoracic cavity pneumothorax	2	Left
2	Rib cage fractures without flail	2	Left posterior rib 5, left posterior rib 6

Case 4: CIREN CASE 658

The 82-year-old, male, belted driver of a Mazda CX3 was impacted at 10 o'clockby a second vehicle, resulting in a delta-v of approximately 18 km/h. Curtain and seat back airbags were activated. The crash occurred at daylight on a two-lane road when the Mazda vehicle was attempting to execute a left turn from a parking lot to join the main road and was impacted by the second vehicle which was traveling on the main road. Pictures of the vehicle are provided in Fig. 7.

The occupant was 180 cm tall and weighed 79 kg. He was seated upright in the middle track position with both hands on the steering wheel. The occupant sustained left posterior rib fractures, a kidney laceration and left pelvic ring fractures. A visual summary of all injuries sustained by the driver is provided in Fig. 8, while Table V provides details about the AIS2+ thoracic and abdominal injuries sustained.

Fig. 7. Pictures of the exterior and interior of the vehicle in Case 4.

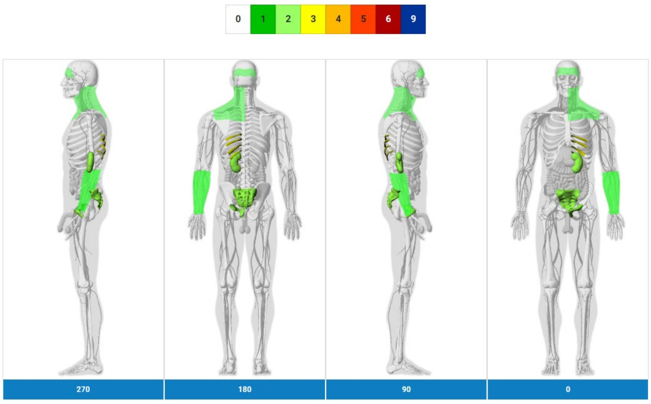

Fig. 8. Summary of injuries sustained by driver in Case 4.

TABLE V

CASE4. DRIVER THORACIC AND ABDOMINAL INJURIES (AIS 2+)

Inj #	Injury Description	AIS Code	Localizer
1	Kidney laceration, minor	2	Left
2	Rib cage fractures without flail	3	Left posterior rib 8, left posterior rib 9, left posterior rib 10,left posterior rib 11

Summary of real-world cases

All the cases reviewed included posterior rib fractures. In Case 1, the posterior rib fractures can be explained by a direct loading of the posterior aspect of the rib cage by the seatback and the impulse transmitted by the unbelted rear occupants. However, in the other cases, posterior rib fractures occurred without a direct loading of the posterior area of the rib cage. In Cases 2 and 3, a compression deformation of the rib cage caused either by the seat belt or the airbags resulted in fractures of the posterior ribs. Case 4 posterior rib fractures were attributed to the contact of the left airbag of the seat back outboard and left door hardware/armrest by the CIREN investigation team. The injury causation scenario notes state that as the fractures were located near the CTv joint, the loading may have been more posterior lateral than pure lateral. However, without knowing the relative position of the subject in the seat it was not possible to completely clarify whether the side airbag deployed against the lateral or the posterior lateral of the torso.

Analyses of PMHS CTs

The analysis of the data obtained from the CTs of the four subjects exhibiting posterior rib fractures shows that the HU measurements of either the CV or CTv joints (or both in several cases) at every vertebral level are substantially higher than the HU measurement corresponding to cancellous bone of the corresponding vertebral level. The HU measurements obtained for each subject at each vertebral level are included in Table VI, and the shaded cells correspond to the observed location of posterior rib fractures in the tests.

Note that consistently, the maximum or the second maximum HU values in either the CV or in the CTv location per vertebral level (except for the single right aspect fracture in subject 02), correspond with the location of one of the posterior rib fractures. This finding suggests a higher risk of posterior rib fracture in joints between the ribs and the spine that are rigidised.

TABLE VI

HU MEASUREMENTS AT EACH THORACIC VERTEBRAL LEVEL. SHADED CELLS SHOW THE RIBS SUSTAINING A POSTERIOR FRACTURE.

Vertebral level	HU body	HU CV right	HU CV left	HU CTv right	HU CTv left
Subject 01					
Vertebral level	HU body	HU CV right	HU CV left	HU CTv right	HU CTv left
T1	179.51	446.53	417.33	166.83	241.35
T2	168.11	212.29	173.93	419.15	335.19
T3	147.07	301.36	268.34	559.70	494.45
T4	204.57	324.23	351.73	516.49	553.51
T5	224.73	263.48	227.71	404.17	641.22
T6	192.45	228.34	160.57	479.46	563.22
T7	209.70	242.45	156.11	566.96	403.27
T8	199.52	176.06	116.23	471.71	408.71
T9	181.22	153.92	133.12	174.93	-
T10	138.42	152.27	178.47	186.99	-
T11	126.05	334.34	370.35	184.99	307.33
T12	113.39	444.88	386.47	-	-
Average	173.73	294.56	358.05	363.22	356.99
SD	35.49	100.77	109.24	163.97	133.18
Subject 02					
Vertebral level	HU body	HU CV right	HU CV left	HU CTv right	HU CTv left
T1	262.48	403.58	306.11	349.52	257.49
T2	203.19	236.94	343.37	230.13	363.20
T3	154.12	161.78	236.60	314.15	236.99
T4	221.41	295.74	322.97	344.57	477.20
T5	183.37	208.08	219.97	489.37	470.39
T6	153	207.56	246.03	427.70	291.37
T7	219.43	376.18	205.39	491.40	349.36
T8	189.75	352.17	213.96	386.67	396.00
T9	260.66	350.92	295.66	429.73	282.89
T10	188.42	223.62	348.34	277.00	-
T11	153.66	299.87	268.50	-	-
T12	126.71	554.57	337.84	-	-
Average	193.02	267.44	295.36	297.93	285.89
SD	42.85	109.61	53.50	87.18	88.15
Subject 03					
Vertebral level	HU body	HU CV right	HU CV left	HU CTv right	HU CTv left
T1	161.27	220.88	339.33	269.56	229.70
T2	172.73	216.65	300.39	217.72	234.88
T3	122.37	361.56	400.44	158.67	156.88
T4	116.16	271.68	392.97	213.69	191.35
T5	147.46	393.31	412.90	169.89	160.35
T6	94.85	202.27	410.45	160.36	184.62
T7	72.36	345.63	418.10	154.83	145.88
T8	59.49	441.97	423.26	162.45	114.65
T9	84.94	430.43	474.36	140.41	176.96
T10	86.50	374.58	348.29	177.63	167.68
T11	53.20	292.36	360.37	115.40	174.76
T12	55.09	371.18	317.60	107.61	123.15
Average	102.20	266.36	346.72	215.31	207.16
SD	41.61	83.84	50.43	45.13	36.42
Subject 04					
Vertebral level	HU body	HU CV right	HU CV left	HU CTv right	HU CTv left
T1	174.06	304.87	447.84	402.94	421.87

T2	196.26	512.08	385.72	279.44	278.57
T3	182.71	392.66	428.18	222.61	270.31
T4	243.81	321.80	367.64	216.05	298.72
T5	275.18	404.08	312.28	273.71	265.71
T6	223.85	323.29	251.45	218.97	178.65
T7	185.70	344.59	249.48	158.74	209.01
T8	198.87	269.72	352.29	234.85	324.78
T9	194.68	312.04	249.26	184.66	337.39
T10	182.54	266.69	285.66	198.24	163.50
T11	176.12	295.73	429.21	187.27	147.90
T12	127.96	262.15	370.67	-	157.59
Average	196.81	403.20	420.58	301.67	323.58
SD	37.30	72.02	73.29	66.65	85.06

Computational Modeling

For each of the four loading conditions analysed, the distribution of strain along each individual rib and the increased risk of fracture of the rib were calculated, in each of the three increased stiffness scenarios described in the methods' section. While the results from all the simulations are included in the Appendix, Fig. 9 and 10 show the outcome of the simulations corresponding to the tests with the rigid impactor impacting on the sternum (Kroell tests, 1971). Figure 9 illustrates how the risk of rib fractures increased when the stiffness of the CV and/or the intervertebral disc was increased. The effect of increasing the stiffness of the CVand intervertebral disc joints is clearly identified in the first and second ribs, while this effect tends to decrease (although it is still present) with increasing rib level.

Figure 10 shows the distribution of maximum principal strain (MPS) along the rib (length of the rib represented in the horizonal axis) bilaterally for the complete rib cage (each row representing a rib level, and each column representing each of the rib cage lateral aspects). It can be seen that increasing the stiffness (regardless of whether it was in the intervertebral disc and/or the CV joint) resulted in increased MPS maximum value. These increased MPS values were more noticeable towards the sections of the ribs that were closer to the spine, regardless of the lateral aspect of the rib cage, as it is easy to identify for ribs 1 and 2 in the figure. A similar effect is also shown in the lower rib levels, especially in rib 12.

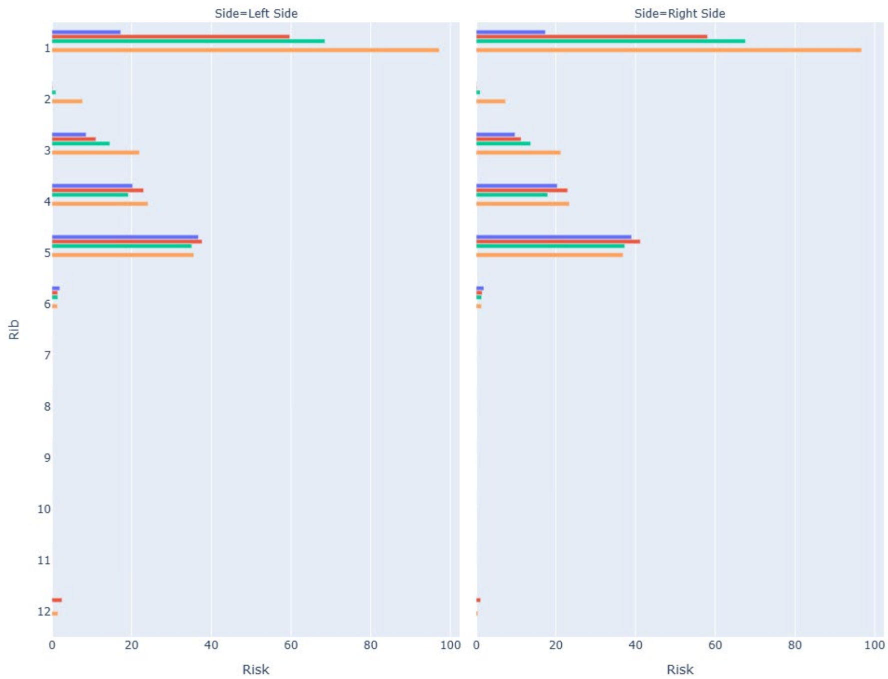

Fig. 9. Risk of rib fracture for the baseline configuration (purple), increased CV joint stiffness (red), increased intervertebral disc stiffness (green) and the effect of stiffening both joints at the same time (orange).

IV. DISCUSSION

The present work combines three different data sources to investigate potential risk factors associated with the occurrence of posterior rib fractures, which are clinically more relevant compared to other rib locations. The goal was to discuss factors that affect the etiology of posterior rib fractures that are different from a direct blow to the posterior rib cage. In some of our PMHS frontal impact tests, a substantial number of posterior rib fractures were identified [22–23] without any loading of the PMHS backs. We therefore explored other factors that could contribute to posterior rib fractures when thoracic loading was primarily due to compression from the three-point seat belt and, in some cases, a driver airbag. Several of these PMHS exhibited spinal osteophytes that rigidised the torso response and limited relative motion between the ribs and the spine. Accordingly, the hypothesis assessed was whether a stiffer rib-spine connection could shift rib deformation and increase the fracture risk in rib regions closer to the spine. If so, since current HBM rib fracture prediction methods are largely based on identifying locations of MPS along the rib [25], accounting for local changes in rib-spine joint stiffness could contribute to a more biofidelic model response.

The influence of the stiffness of the joint in how the rib cage deforms should be considered also in the assessment of potential injury mechanisms. In the parametric study carried out with the VIVA+ HBM, we have included four different loading conditions (a belted frontal impact, a pure frontal and a pure lateral impactor test, and a table-top test conditions) in which the main loading mechanism of the chest was compression. In all of them, the increase of the stiffness in the CV joint resulted in increased risk of posterior rib fractures suggesting that these fractures can occur even if the main loading mechanism of the chest is compression.

Last, this paper presents a unique perspective of contributing factors combining real-world data from across the world (India, US) and a collaboration with a European institution. There are not that many real-world databases that can provide the level of injury detailed needed in this paper. Some of the authors are members of the RASSI team and CIREN provides public access to its records. Thus, the selection of these two data sources was motivated by the accessibility of the data. Despite showing some commonalities (for instance, high delta-V cases and belted injured drivers) across the two countries, the study also indicated that regional differences in real-world collisions need to be considered when analysing potential injury mechanisms. The characteristics of the selected crashes in India compared to the ones in the US were completely different, even though they resulted in similar thoracic injury patterns. Thus, the same injury outcome was caused by different injury mechanisms. While the cases in India show unbelted rear occupants (belt use was about 75% for drivers but less than 10% for rear seat occupants [26]), younger occupants' age, absence of airbags, probably lack of stiffness of the front seat seatback and issues of compatibility between vehicles of very different sizes (mass ratio in Case 1 was 12:1 between the two vehicles, while research has shown that typically in Europe and the US this ratio is close to 1:1, [27]), the two cases in the US resulted in a similar pattern of thoracic injuries caused by a more distributed loading of the chest provided by the airbags. Thus, the strategies for an effective reduction of posterior rib fractures need to be different and include these regional differences.

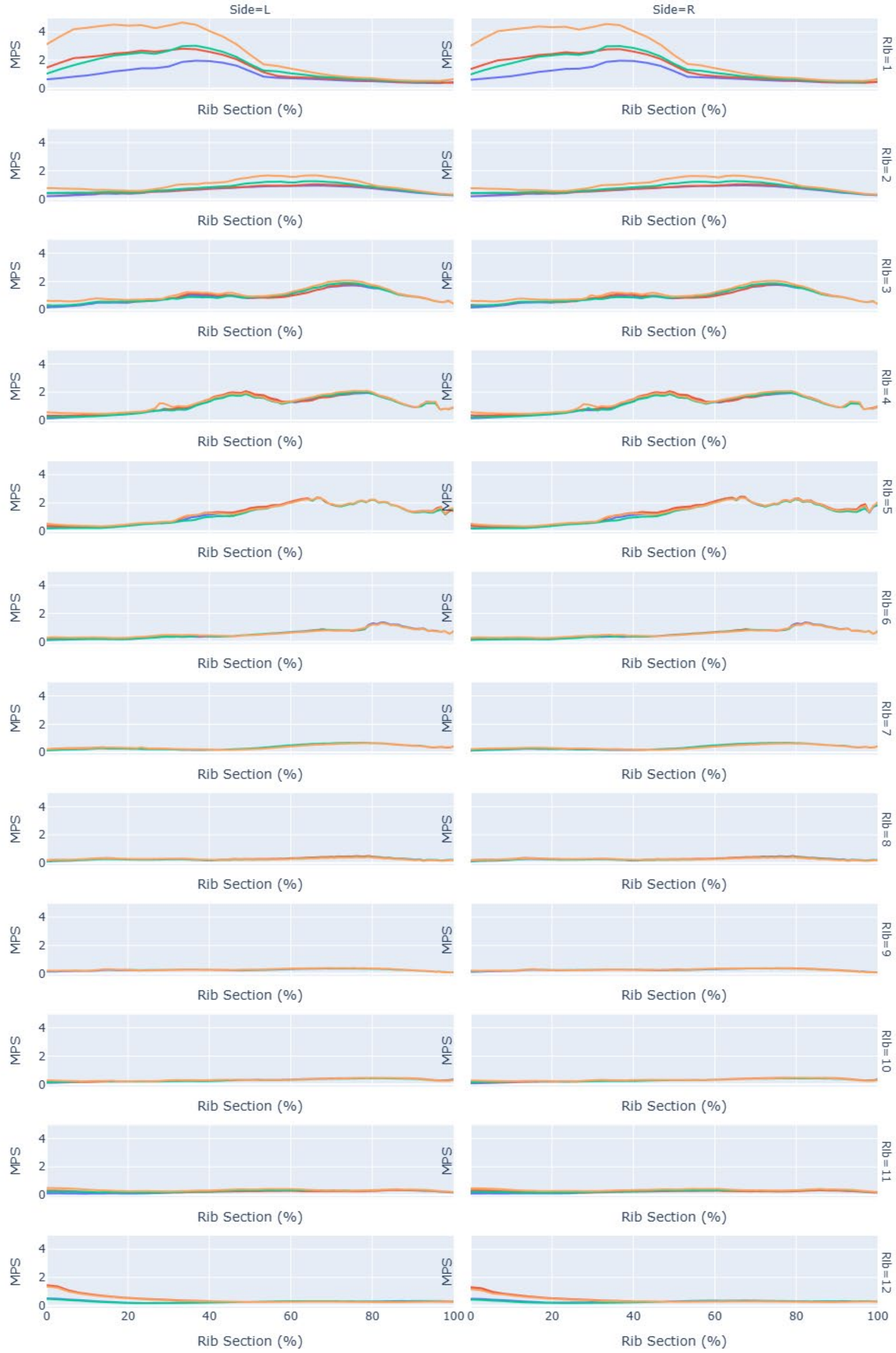

Fig. 10. Comparison of MPS along the length of the rib in the Kroell tests (1971) for four stiffness conditions: baseline (purple), increased stiffness in CV joint (red), increased stiffness between vertebral bodies (green), combination of increased stiffness in CV joint and vertebral bodies (orange). CV joint corresponds to 0% Rib Section and costosternal joint corresponds to 100% Rib Section.

This study has several limitations. The descriptive analysis of real-world data is limited to a few selected cases. This convenience sample was chosen to identify crashes resulting in posterior rib fractures caused by different injury mechanisms. Its purpose was not to draw conclusions that could be extrapolated to the whole crash population in the US or India, but to confirm that posterior rib fractures can occur without direct contact to the posterior rib cage and that compressive deformation of other rib cage regions can result in fracture of the posterior rib area. The CT analysis included only cases with posterior rib fractures. Again, this analysis was not intended to provide a robust conclusion that CTv and CV joint stiffness causes posterior rib fractures, but rather to serve as an exploratory study guiding the design of the computational modelling experiments. While in the autopsy of the PMHS and in CIREN cases it was possible to identify the exact location of the rib fractures, the identification of posterior rib fractures in RASSI was obtained from the L1 localizer of AIS codes, which do not contain information about which individual ribs were fractured.

V. CONCLUSION

This study combined real-world crash investigations, PMHS computed tomography analyses, and computational modeling to examine potential factors contributing to posterior rib fractures. Across these three data sources, the findings consistently suggest that posterior rib fractures are not exclusively associated with a direct blow to the posterior thorax. In the case series, posterior fractures were observed both in scenarios involving direct posterior loading and in crashes in which thoracic compression from the restraint system and surrounding structures appeared to be the dominant loading mode. In the PMHS analyses, posterior fracture locations tended to coincide with elevated Hounsfield unit values at the costovertebral and costotransverse joints, suggesting increased local ossification or rigidity. In the VIVA+ sensitivity study, increasing stiffness at the rib-spine articulations and adjacent thoracic joints shifted strain toward posterior rib regions and increased model-predicted fracture risk. Taken together, these observations support the hypothesis that increased stiffness of the thoracic spine-rib complex may predispose occupants to posterior rib fractures during compressive thoracic loading. However, the present study is exploratory and does not establish causality. Future work should include larger case series, comparison with non-posterior-fracture controls, quantitative characterisation of joint degeneration, and calibration of subject-specific joint stiffness in human body models. Such work may improve the biomechanical interpretation and prediction of posterior rib fractures in restrained occupants.

VI. REFERENCES

[1] Liebsch, C., Seiffert, T., Vlcek, M., Beer, M., Huber-Lang, M. and Wilke, H.-J. (2019) Patterns of serial rib fractures after blunt chest trauma: An analysis of 380 cases. *PLOS ONE*, **14**(12): p.e0224105.

[2] Hulse, C. N., Stull, K. E. and Weaver, A. (2019) Rib fracture frequency and location using vehicular crash data. *Forensic Anthropology*, **2**(1): pp.1–8.

[3] Lee, E. L., Craig, M. and Scarboro, M. (2015) Real-world rib fracture patterns in frontal crashes in different restraint conditions. *Traffic Injury Prevention*, **16**(sup2): pp.S115–S123.

[4] Kim, W., Lee, J., Kim, S., Park, J., Kim, Y., Lee, S. and *et al.* (2023) Characteristics of rib fracture patients who require chest computed tomography in the emergency department. *BMC Emergency Medicine*, **23**(1): p.33.

[5] Flagel, B. T., Luchette, F. A., Reed, R. L., Esposito, T. J., Davis, K. A., Santaniello, J. M. and *et al.* (2005) Half-a-dozen ribs: The breakpoint for mortality. *Surgery*, **138**(4): pp.717–725.

[6] Chen, X.-K., Sun, L., Yu, Z.-Q., Wang, Y., Li, Y.-B. and Zhang, H. (2020) Assessment of thoracic volume changes after the collapse of lateral rib fractures based on chest computed tomography data: Computer simulation and a multiple variable linear regression analysis. *Journal of Cardiothoracic Surgery*, **15**(1): p.167.

[7] Martin, T. J., Eltorai, A. E. M., Dunn, R., Varone, A., Joyce, M. F. and Daniels, A. H. (2019) Clinical management of rib fractures and methods for prevention of pulmonary complications: A review. *Injury*, **50**(6): pp.1159–1165.

[8] Pieracci, F. M., Majercik, S., Ali-Osman, F., Ang, D., Doben, A., Edwards, J. and *et al.* (2017) Surgical stabilization of rib fractures: Rib fracture colloquium clinical practice guidelines. *Injury*, **48**(2): pp.307–321.

[9] Bauman, Z. M., Ruggero, J., Powell, J., Dunne, J., Shapiro, M. and Cotton, B. (2021) Rib fracture displacement worsens over time. *European Journal of Trauma and Emergency Surgery*, **47**(6): pp.1965–1970.

[10] Lin, F. C.-F., Li, R.-Y., Tung, Y.-W., Jeng, K.-C. and Tsai, S. C.-S. (2016) Morbidity, mortality, associated injuries, and management of traumatic rib fractures. *Journal of the Chinese Medical Association*, **79**(6): pp.329–334.

[11] Ziegler, D. W. and Agarwal, N. N. (1994) The morbidity and mortality of rib fractures. *Journal of Trauma*, **37**(6): pp.975–979.

[12] Crandall, J. R., Kent, R. W., Patrie, J. T., Fertile, J. and Martin, P. G. (2000) Rib fracture patterns and radiologic detection – A restraint-based comparison. *Proceedings of the Association for the Advancement of Automotive Medicine*, **44**: pp.235–260.

[13] Ranmal, A., Shaikh, J. and Lubbe, N. (2024) Rib and sternum fracture risks for restrained occupants in frontal car crashes. *Traffic Injury Prevention*, **25**(4): pp.616–622.

[14] Kent, R., Lessley, D., Sherwood, C., Forman, J., Parent, D. and Crandall, J. (2005) Structural and material changes in the aging thorax and their role in crash protection for older occupants. *Proceedings of the Stapp Car Crash Conference*, 2005, San Diego, USA.

[15] Liebsch, C. and Wilke, H.-J. (2022) How does the rib cage affect the biomechanical properties of the thoracic spine? A systematic literature review. *Frontiers in Bioengineering and Biotechnology*, **10**: p.900048.

[16] Padmanaban, J., Ravishankar, R. and Dandapani, A. (2017) Methodology to derive national estimates of injuries and fatalities in road traffic crashes in India. *SAE Technical Paper Series*, 2017.

[17] Lopez-Valdes et al. (2024). The impact response of four PMHS to frontal impacts in reclined positions. *Proceedings of the IRCOBI Conference*, 2024, pp. 232–233.

[18] J. Uriot et al., "Reference PMHS sled tests to assess submarining," SAE Technical Paper, no. Journal Article, 2015.

[19] Crandall, J. R. (2012) ATD thoracic response test development, gold standard buck condition 2: Force-limited belt, 30 km/h frontal, PMHS 494 and 492. National Highway Traffic Safety Administration, Report No. DTNH22-09-H-00247, Washington, DC.

[20] Kroell, C. K., Schneider, D. C. and Nahum, A. M. (1971) Impact tolerance and response of the human thorax. In: Backaitis, S. H. (ed.) *Biomechanics of Impact Injury and Injury Tolerances of the Thorax–Shoulder Complex*. SAE, Warrendale, PA.

[21] Viano, D. C., Lau, I. V., Asbury, C., King, A. I. and Begeman, P. (1989) Biomechanics of the human chest, abdomen, and pelvis in lateral impact. *Accident Analysis and Prevention*, **21**(6): pp.553–574.

[22] Kent, R., Lessley, D. and Sherwood, C. (2004) Thoracic response corridors for diagonal belt, distributed, four-point belt, and hub loading. *Stapp Car Crash Journal*, **48**: pp.449–470.

[23] John, J., Klug, C., Kranjec, M., Svenning, E. and Iraeus, J. (2022) VIVA+: A human body model lineup to evaluate sex-differences in crash protection. *Frontiers in Bioengineering and Biotechnology*, **10**: p.918345.

[24] Lopez-Valdes, F. J., Kent, R. W., Forman, J. L., Lessley, D. J., Gepner, B. and Parent, D. (2018) Chest injuries of elderly postmortem human surrogates under seat belt and airbag loading in frontal sled impacts: Comparison to matching THOR tests. *Traffic Injury Prevention*, **19**(sup2): pp.S55–S63.

[25] Lopez-Valdes, F. J., Kent, R. W., Forman, J. L., Lessley, D. J., Gepner, B. and Parent, D. (2024) The impact response of four postmortem human surrogates to frontal impacts in reclined positions. Proceedings of the IRCOBI Conference, 2024, Cambridge, UK, pp.232–233.

[26] Forman, J. L., Kent, R. W., Mroz, K., Pipkorn, B., Boström, O. and Segui-Gomez, M. (2012) Predicting rib fracture risk with whole-body finite element models: Development and preliminary evaluation of a probabilistic analytical framework. *Annals of Advances in Automotive Medicine*, **56**: pp.109–124.

[27] Marketing & Development Research Associates (2020) Observations of helmet and seat belt wearing by motorised two-wheeler and car users. JP Research Inc., New Delhi.

[28] Padmanaban, J., Delahaye, M., Hassan, A. M. and Mackay, M. Problems with comparing vehicle compatibility issues in US and UK fleets. *Proceedings of the IRCOBI Conference*, 2004, Graz, Austria. pp.13–24.

APPENDIX

Additional information from real-world cases

Case 1: RASSI 91-2019-002—0113

Crash Scene and Events: Unit 1 (Maruti Suzuki Wagon-R Zxi, Car, 5 Occupants) was travelling from south-west to north-east on left lane of the two-lane undivided national highway. Unit 2 (TATA Motors 1109H EX2, Truck 2 Occupants) was travelling from north-east to south-west on left lane of the roadway. Unit 1 Car driver fell asleep and entered the oncoming lane. Unit 1 had a head on impact with Unit 2. Post impact, Unit 1 was pushed backward by Unit 2 for some distance and went off-road towards left side of road in a ditch and Unit 2 travelled some distance ahead point of impact. 5 occupants of Unit 1 were fatal on the scene. Both occupants of Unit 2 were unharmed.

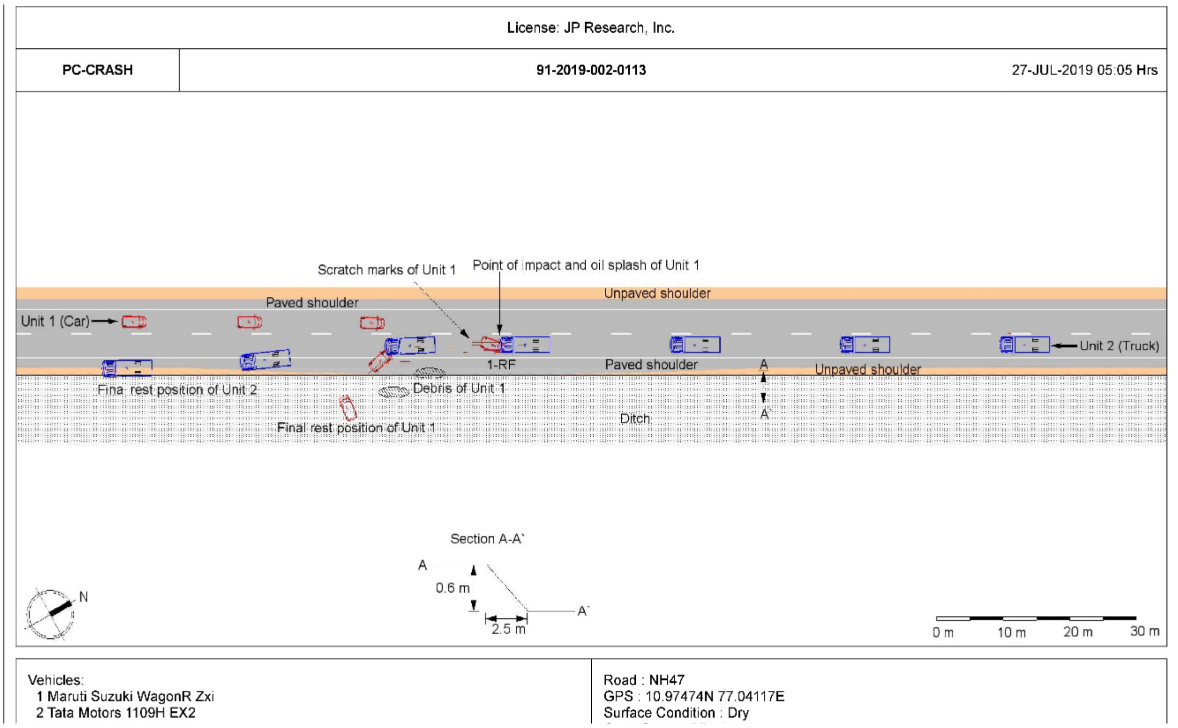

Fig A. 1 Sketch of the collision

Vehicles details

Data point	***Car***	***Truck***
Kerb Weight (kg)	1340	12990
No. of occupants	4	1
Travel speed (kmph)	39	54
Impact speed – 1*st* collision (kmph)	39	54
Delta-v (kmph)	90	8
Direction of Force (1*st* collision)	01 O'Clock	12 O'Clock
General Area of Damage (1*st* collision)	Front	Front

Case 2: RASSI 91-2023-011-0196

Crash Scene and Events: Unit 1 (Maruti Suzuki Zen VX, Hatchback, 4 Occupant) was travelling from north-east to south-west. The road structure is four lanes divided (Median with raised curb and metal fence with two lanes service on both sides) national highway. Unit 1 was travelling straight in left most lane. Due to unknown reason driver of unit 1 lost control and went towards left and impacted manhole on front plane (Event 1). Post that, unit 1 rolled over on right plane (Event 2). Unit 1 completely stopped and rested on top plane. All four occupants of unit 1 were transported to hospital by ambulance. Unit 1 driver declared fatal during the treatment meanwhile other three occupants sustained minor injuries.

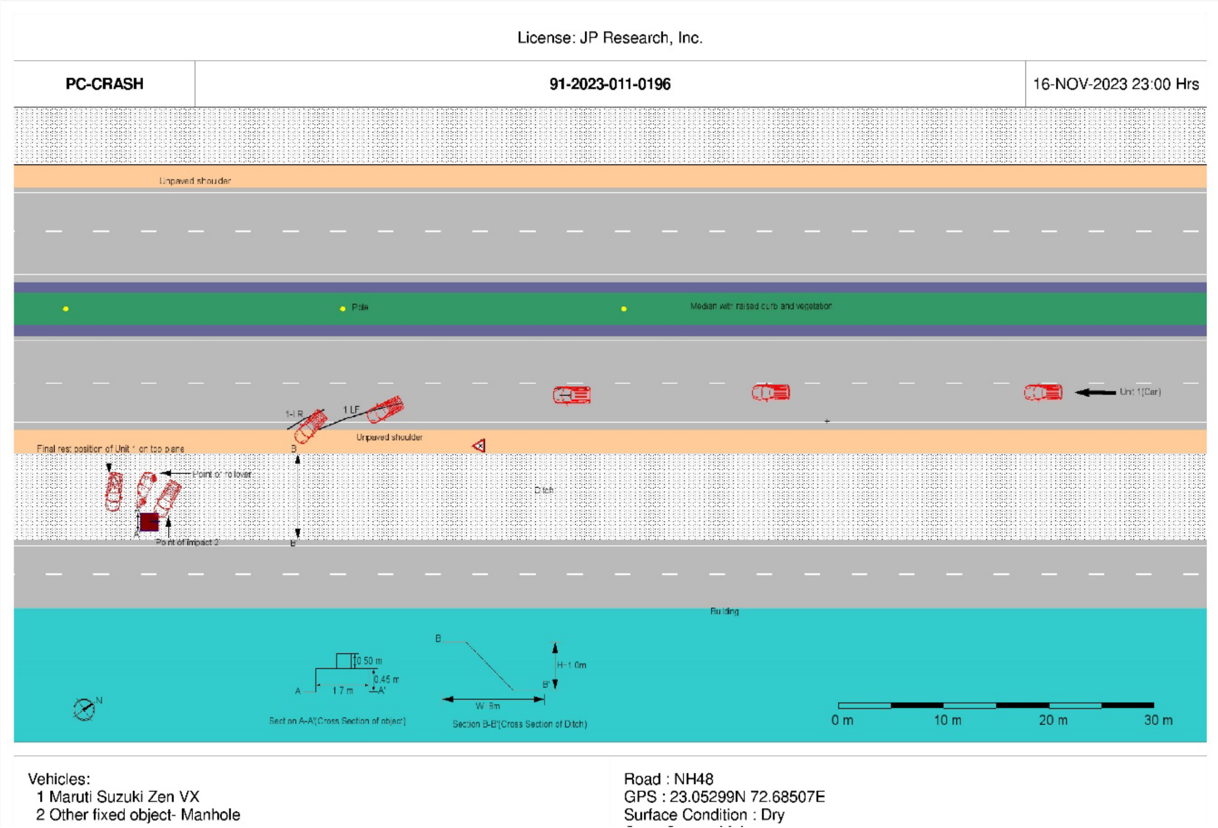

Fig A. 2 Sketch of the collision

Vehicle details

Data point	Car
Kerb Weight (kg)	765
No. of occupants	4
Travel speed (kmph)	68
Impact speed – 1st collision (kmph)	32
Delta-v (kmph)	999999
Direction of Force (1st collision)	12 O'Clock
General Area of Damage (1st collision)	Front

Case 3: CIREN CASE 584

Crash Scene and Events: Vehicle 1 drifted over the centre lane line and onto the left roadside where it struck a large 60 cm diameter tree (Event 1) with its left plane then continued a short distance and struck an 80 cm diameter tree with its front plane (Event 2). After impact, the vehicle rotated counterclockwise and came to rest at the 80 cm diameter tree while remaining on the roadside facing southeast.

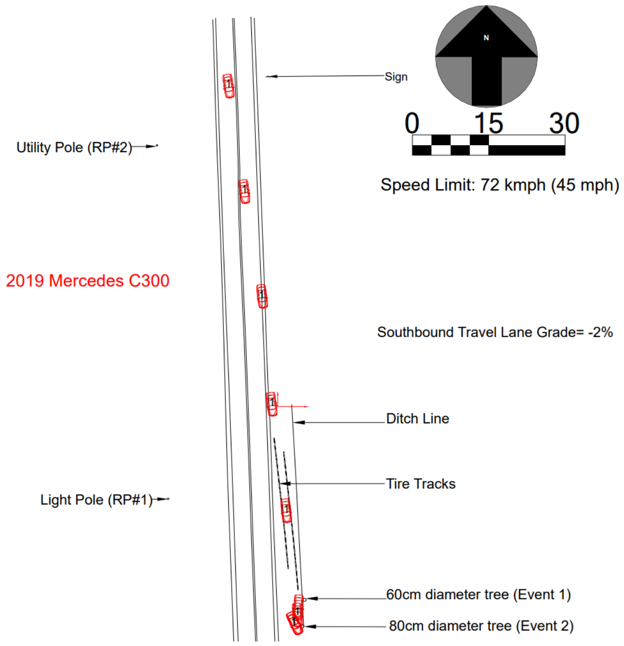

Fig A. 3 Sketch of the collision

Case 4: CIREN CASE 658

Crash scene and events: the crash occurred during daylight hours on a dry, bituminous, two-lane roadway under clear skies. There was one northbound travel lane and one southbound travel lane with speed limit of 40 km/h (25 mph). The northbound lane had a -3.6 percent grade slope and the southbound lane had a +3.6 percent grade. Both travel lanes were divided by a double yellow line.

A 2016 Mazda CX-3 (V1) was in a parking lot attempting to execute a left turn to travel south. A 2011 Dodge Charger (V2/police car) was traveling north responding to an emergency call with lights sirens activated. V1 was in a parking lot (facing west) and attempted to enter the roadway intending to turn left. As V1 entered the roadway it was impacted on the left side by the front of V2 (Event 1). V1 then rotated counterclockwise and traveled off the west road edge and impacted an embankment with its front left bumper (Event 2). After initial impact V2 continued on in a northern direction and traveling to final rest approximately 40 meters north of impact area facing north in the middle of the roadway. V1 and V2 were towed from the scene due to damage.

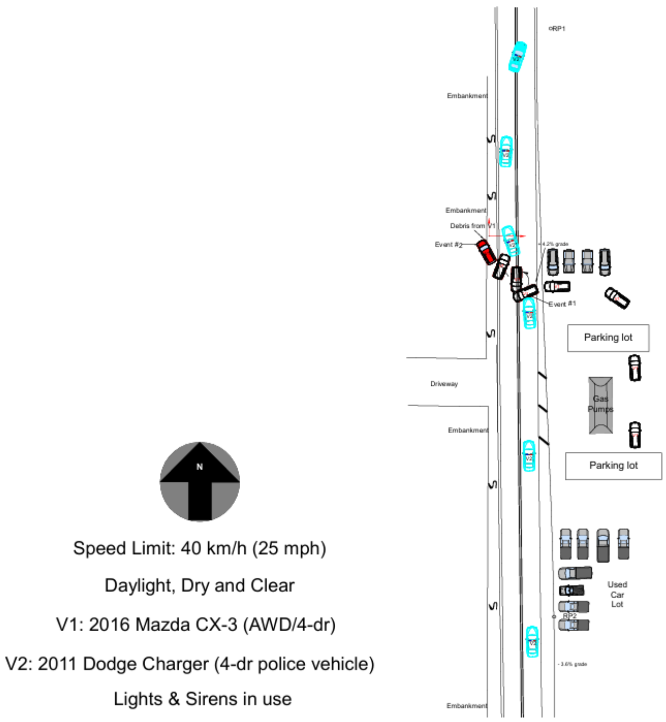

Fig A. 4 Sketch of the collision

Rib anatomy

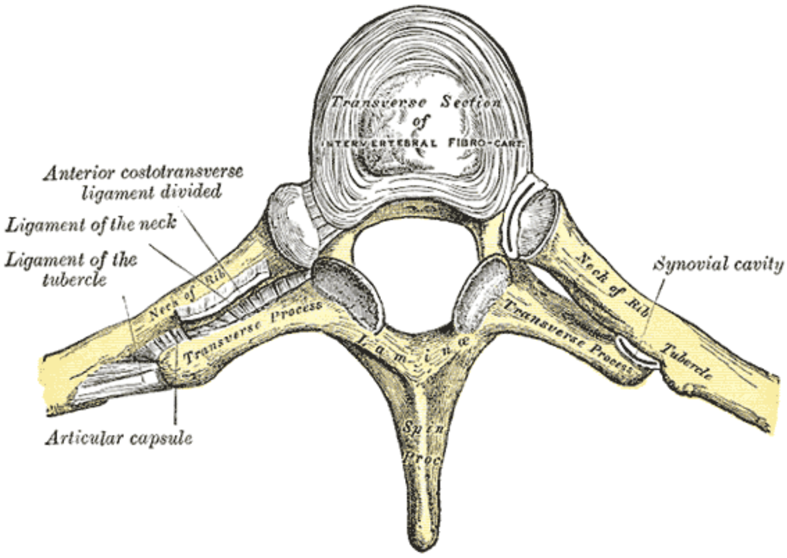

Fig A. 5 Anatomy of the rib with the costotransverse and costo-vetebral (at the end of the neck of the rib) joints. By Henry Vandyke Carter - Henry Gray (1918) Anatomy of the Human Body (See "Libro" section below)Bartleby.com: Gray's Anatomy, Plate 313, https://commons.wikimedia.org/w/index.php?curid=85402

Computer simulation results from all the load cases simulated

The load cases used in the computational study are shown in the following figure.

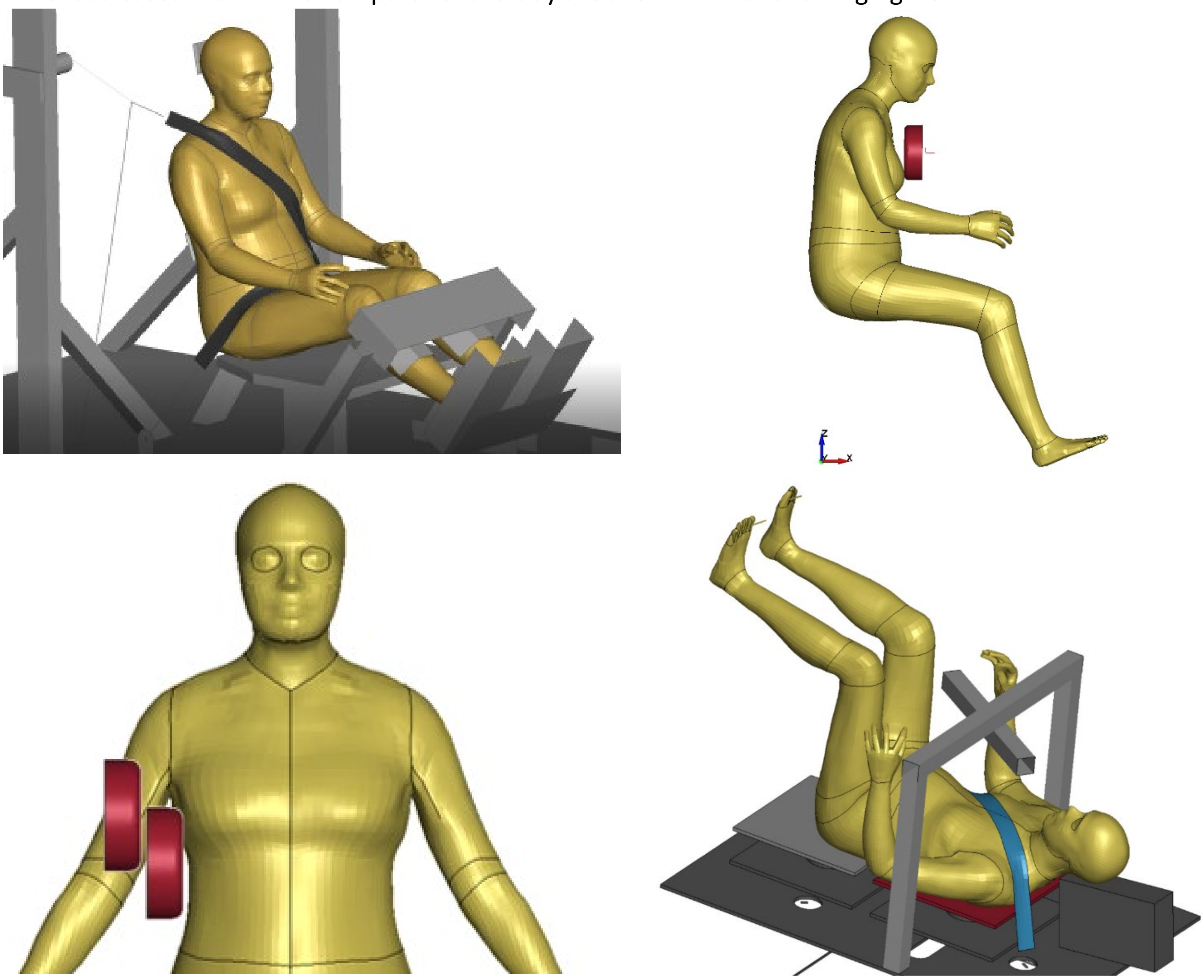

Fig A. 6 Load cases used in the computational study. From left to right and top to bottom: Gold-standard tests (Crandall et al. 2011), frontal impactor tests (Kroell et al. 1971), lateral impact (Viano 1989) and table-top tests (Kent et al. 2004)

Gold-standard tests (Crandall et al. 2011)

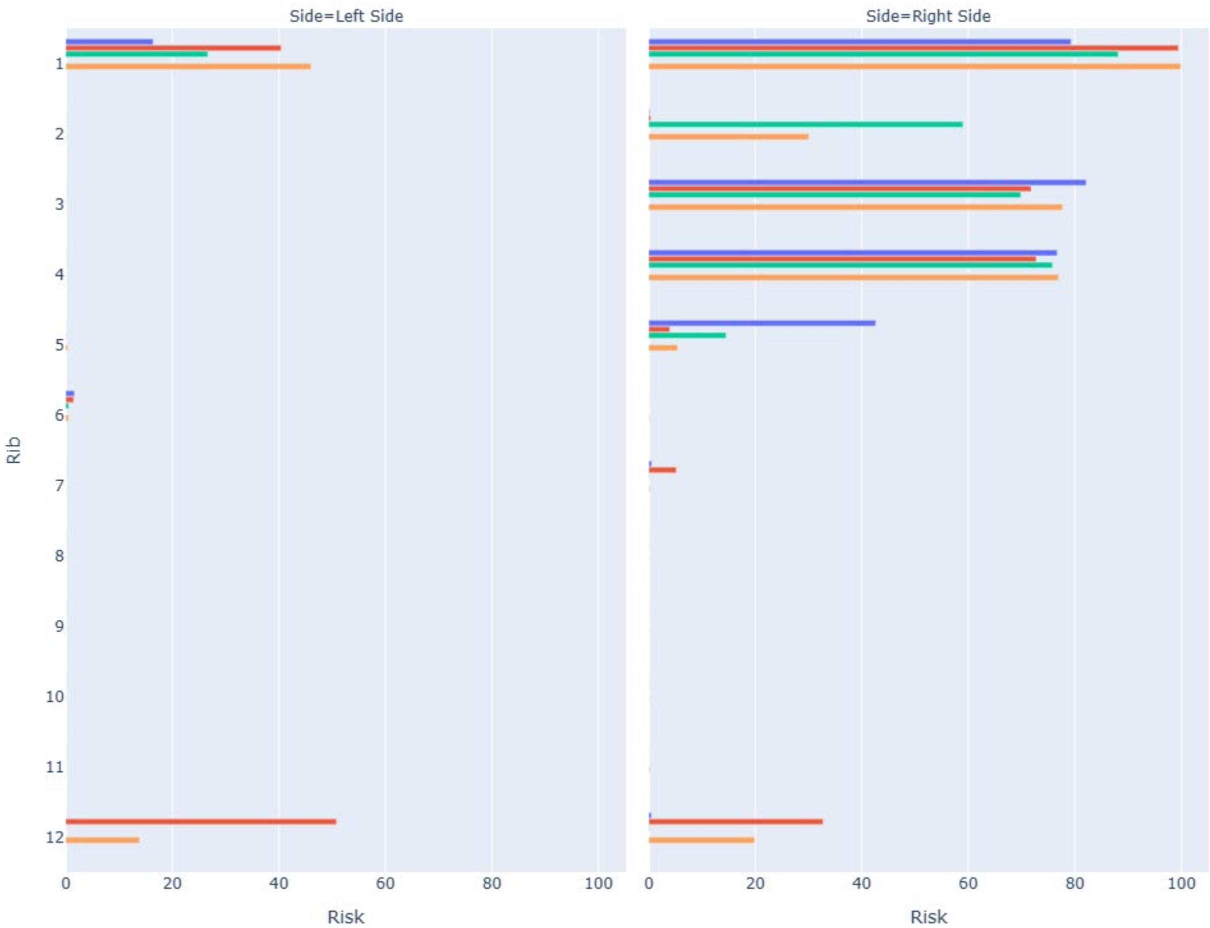

Fig A. 7 Risk of rib fracture for the baseline configuration (purple), increased CV joint stiffness (red), increased intervertebral disc stiffness (green) and the effect of stiffening both joints at the same time (orange).

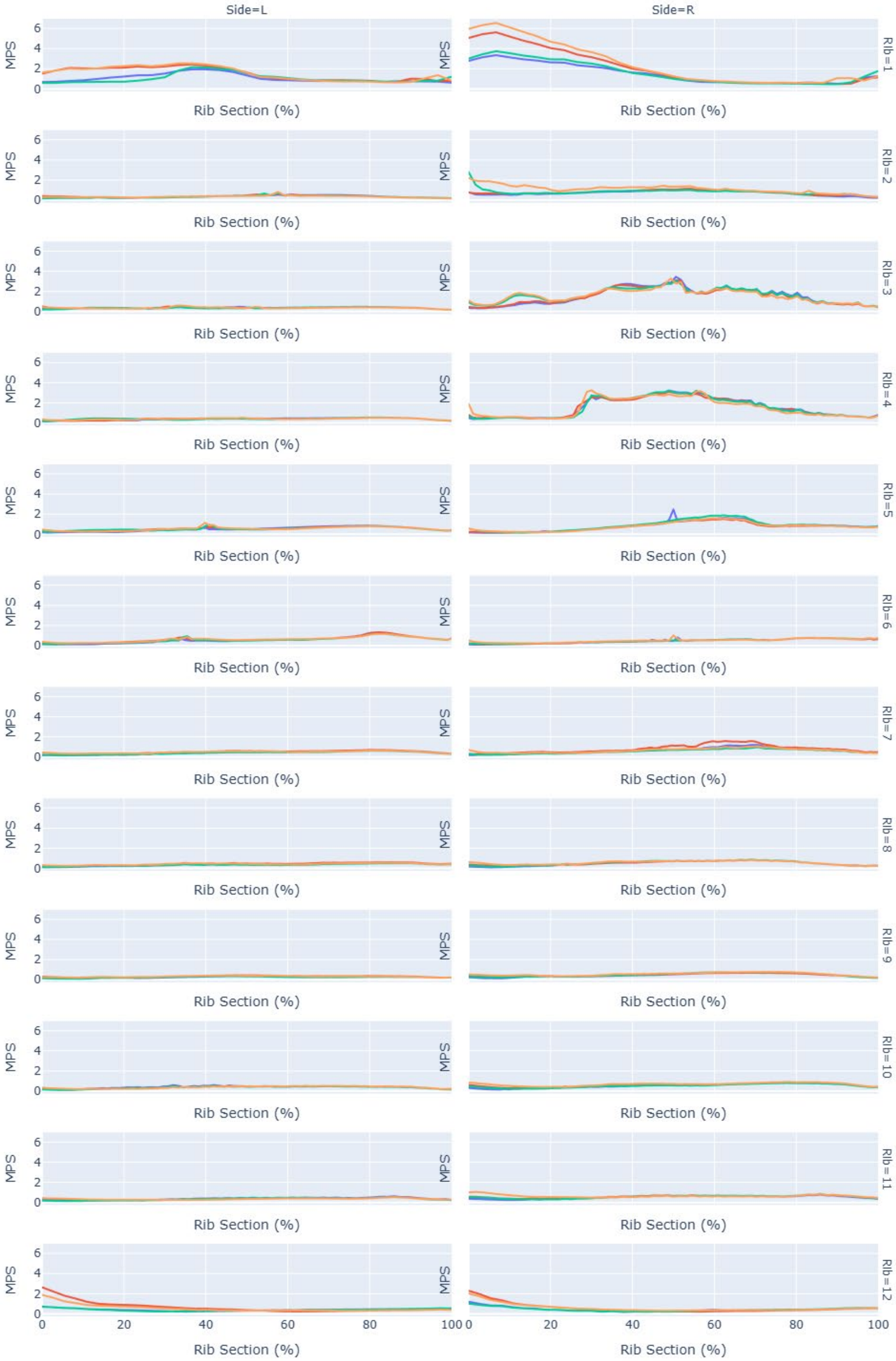

Fig A. 8 Comparison of MPS along the length of the rib in the Crandall tests (2011) for four stiffness conditions: baseline (purple), increased stiffness in CV joint (red), increased stiffness between vertebral bodies (green), combination of increased stiffness in CV joint and vertebral bodies (orange)

Lateral impactor (Viano, 1989)

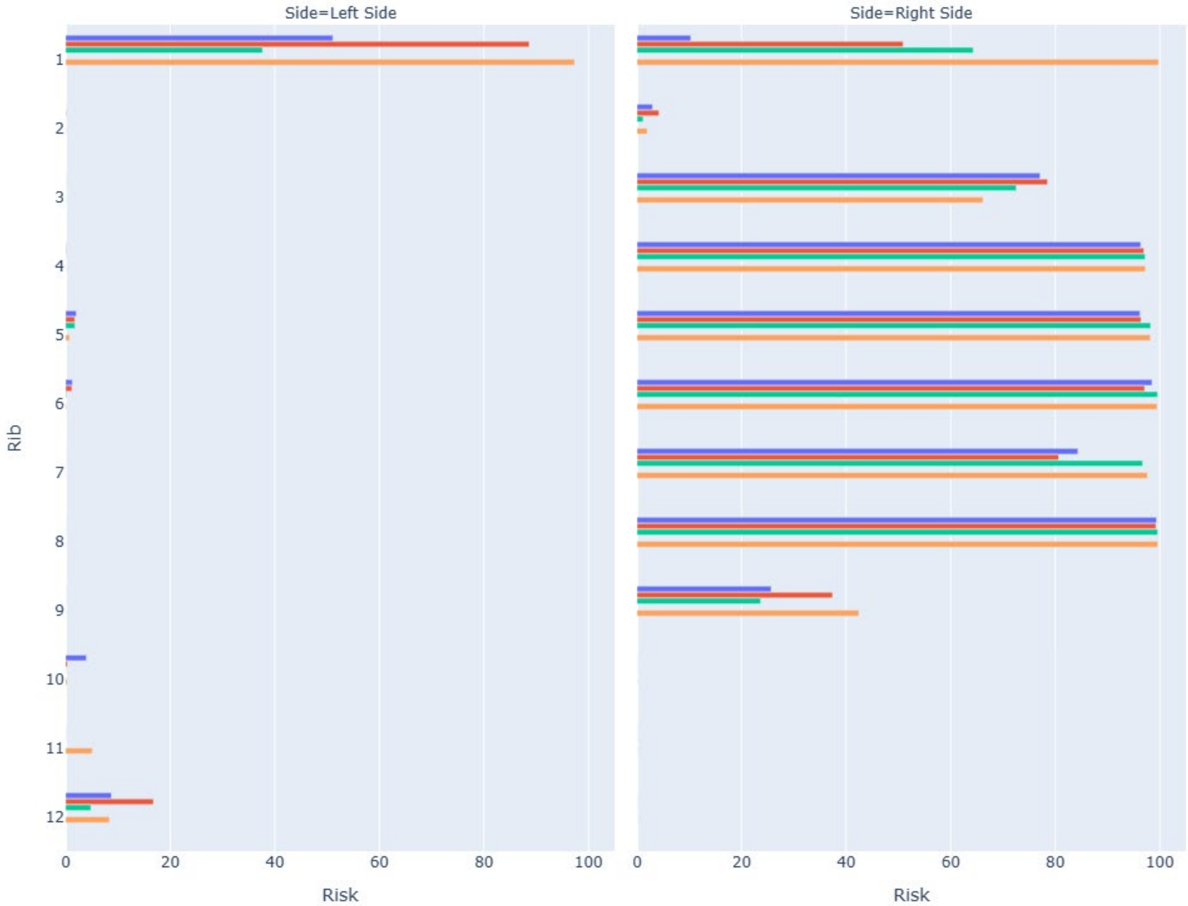

Fig A. 9 Risk of rib fracture for the baseline configuration (purple), increased CV joint stiffness (red), increased intervertebral disc stiffness (green) and the effect of stiffening both joints at the same time (orange)

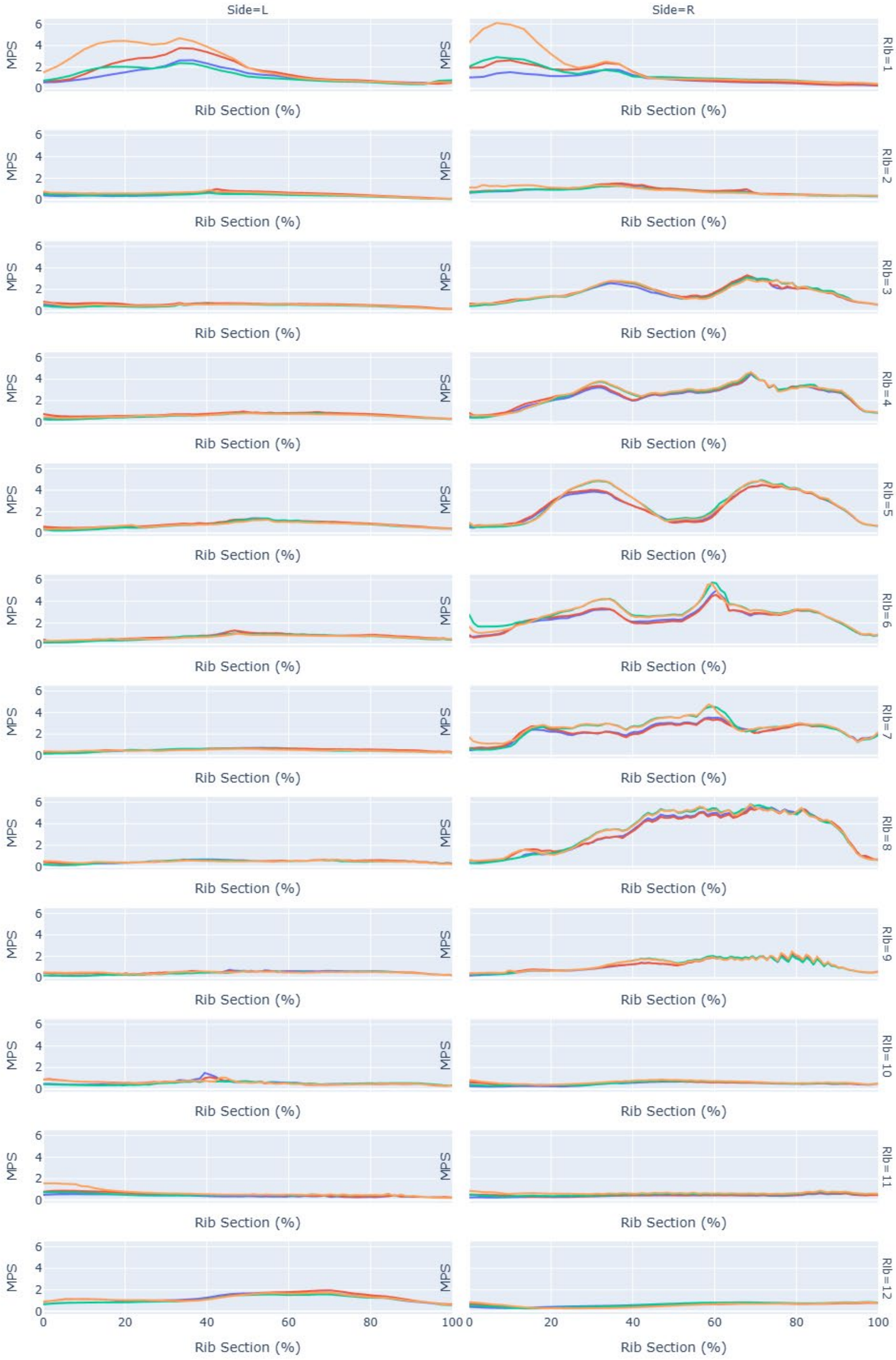

Fig A. 10 Comparison of MPS along the length of the rib in the Viano tests (1989) for four stiffness conditions: baseline (purple), increased stiffness in CV joint (red), increased stiffness between vertebral bodies (green), combination of increased stiffness in CV joint and vertebral bodies (orange)

Table top tests (Kent et al.2004)

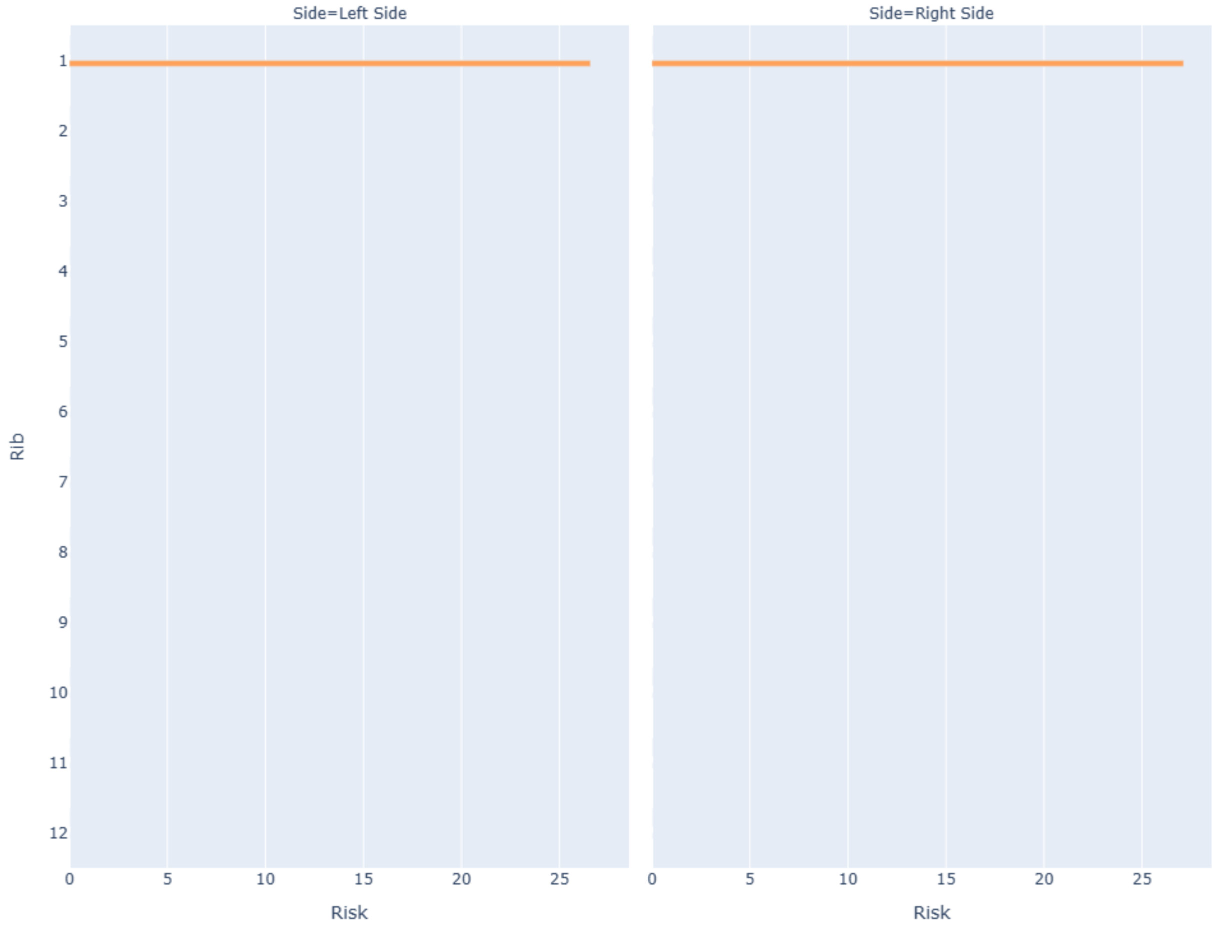

Fig A. 11 Risk of rib fracture for the effect of stiffening both joints at the same time (orange). Note that the rib fracture risk for any of the other conditions (baseline, increased CV joint stiffness, increased IV disc stiffness) was minimal (nearly zero) for all vertebral levels.

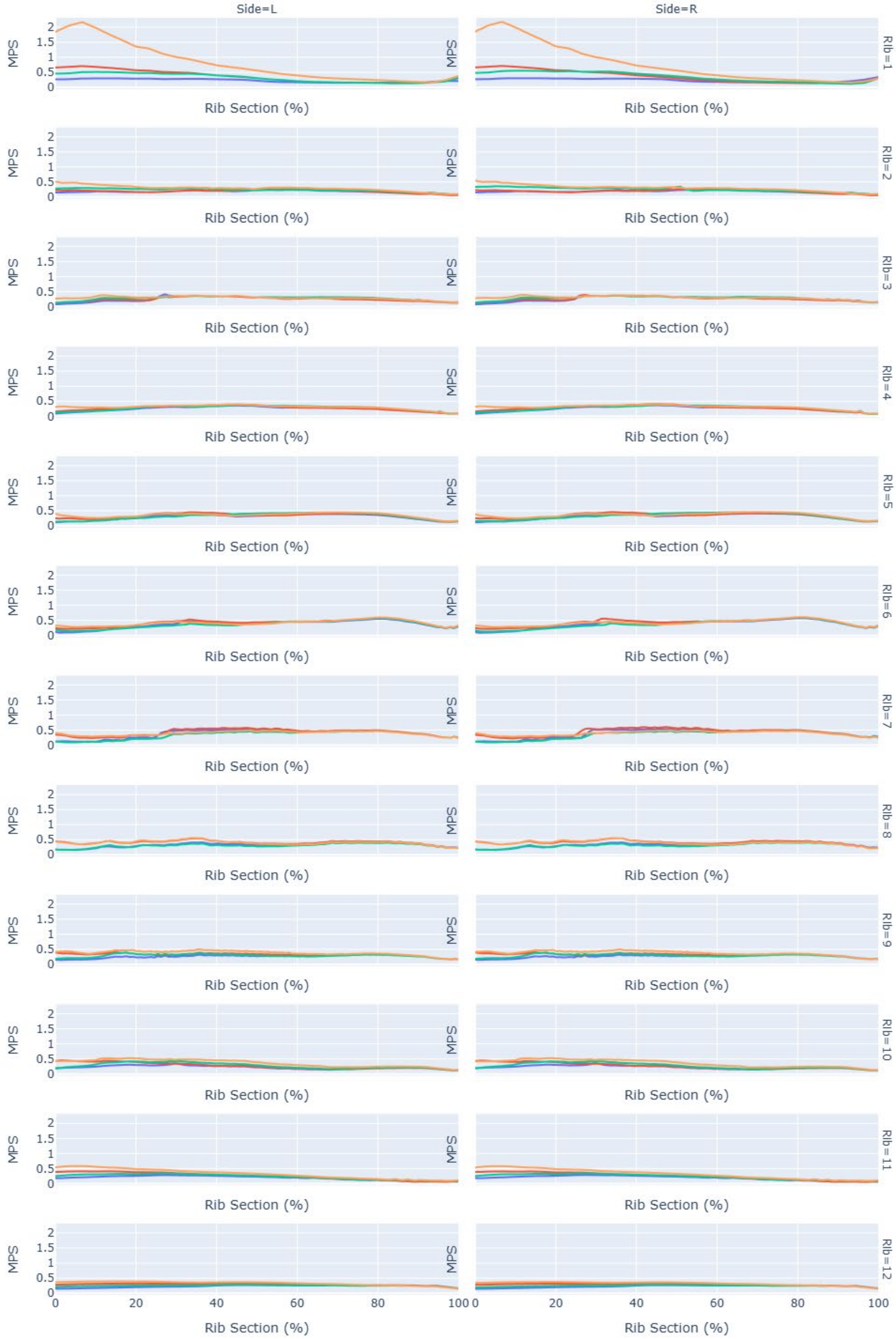

Fig A. 12 Comparison of MPS along the length of the rib in the top-table tests (Kent *et al*. 2004) for four stiffness conditions: baseline (purple), increased stiffness in CV joint (red), increased stiffness between vertebral bodies (green), combination of increased stiffness in CV joint and vertebral bodies (orange)